NIRC2 Geometric Distortion

P. Brian Cameron, Caltech

1. Summary

Here we compute a new solution for the geometric distortion in the wide (40 mas/pixel) and narrow (10 mas/pixel) cameras of NIRC2. We find the post-fit residuals are improved by a factor of 6–8 over the previous (pre-ship) solution with magnitudes $\lesssim 0.1$ pixels (1-σ). There is still some small scale structure in the residuals indicating that a higher order solution may be necessary. We also include a comparison with the previous solution.

2. Introduction

All optical systems suffer from some type of geometric distortion. Here we will characterize this distortion for the NIRC2 camera behind the AO system at the Keck II telescope.

A solution for all three NIRC2 cameras was derived from images of grid of holes drilled in fused silica to simulate a known reference grid (which will refer to also as the pin hole mask; Figure 1). The current distortion solutions for each camera have a polynomial expression in the form

$$x' = a_0 + a_1 x + a_2 y + a_3 x^2 + a_4 xy + a_5 y^2 + a_6 x^3 + a_7 x^2 y + a_8 x y^2 + a_9 y^3, \quad (1)$$

$$y' = b_0 + b_1 x + b_2 y + b_3 x^2 + b_4 xy + b_5 y^2 + b_6 x^3 + b_7 x^2 y + b_8 x y^2 + b_9 y^3, \quad (2)$$

where

$$x = x_{\rm obs} - 512, \quad (3)$$

$$y = y_{\rm obs} - 512. \quad (4)$$

Here $x_{\rm obs}$ and $y_{\rm obs}$ are the observed locations of the pin holes, whereas x' and y' are their positions after correcting for the geometric distortion (i.e. their 'true' positions in a distortion free system).

One minor point, there is an inconsistency with this solution. First, the the center of the array ($x_{\rm obs} = 512, y_{\rm obs} = 512$) is, by definition, free of distortion. However, fitting for the constants a_0, b_0 shifts a star at 512,512 from the center of the array. In reality, these coefficients just represent an overall shift of the pin hole image, so they should be dropped when applying the solution.

The pre-ship solution can be found in Table 1 (Thompson et al.) and is shown graphically for the wide camera in Figures 4 & 5 and in Figures 10 & 11 for the narrow camera. The post-fit residuals after applying this pre-ship solution were reported as $(\sigma_x, \sigma_y) = (0.57, 0.29)$ for the wide

camera and $(\sigma_x, \sigma_y) = (0.81, 0.62)$ for the narrow camera (Thompson et al. 2001[1]). Our goal is to improve these values.

3. Data

We will consider two data sets for determining the wide (40 mas/pixel) and narrow (10 mas/pix) camera solutions (the medium resolution camera is used rarely for imaging). The wide camera data set consists of 5 images of the illuminated pin hole mask taken with 5 second integrations and 4 on chip coadds. The data were taken on 2006 Dec 20 UT. The narrow camera consists of 10 images with 20 seconds exposure times and 3 coadds taken on 2006 Nov 29 UT. The data have images taken at two different dither positions separated by $\sim 1/2$ a hole spacing. Both data sets are after the large earthquake to hit Hawaii in 2006 Oct. A diagram of the pin hole mask is seen in Figure 1, and has an expected hole separation of 24.25 pixels in the wide camera and 48.41 pixels in the narrow. An image of the coarse grid with the wide camera can be seen in Figure 2. The slit wheel can't quite move the coarse grid over the entire chip, thus we can only characterize the region of $x \sim [0 : 800]$. The difference image of the fine grid at two positions with the narrow camera can be seen in Figure 3.

4. Analysis

The data reduction is straight forward. First we linearize the frames according the the prescription of Stan Metchev [2], then flat field with dome flats. The leakage of light from the lamps in the AO bench (used to illuminate the mask) is significant and leads to a gradient across the chip. Moving the pin hole mask by $\sim 1/2$ the hole spacing is effective for narrow camera, but doesn't yield good background subtraction for the wide camera.

The next step is to derive the observed positions for the pin holes. We do this by fitting a position dependent (quadratically varying) PSF to the pin hole sources (to account for the variable image quality across the field, although simple centroiding yields consistent results). We will refer to these as $x_{\rm obs}$ and $y_{\rm obs}$.

The above steps are straightforward, but deriving the *expected* pin hole positions for comparison is more difficult. It is clear from Figure 2 that the grid has some rotation with respect to the $x - y$ axes of the NIRC2 detector. Also, the prediction of the hole spacing on the detector rests on the assumption of detector pixel scale, which could be variable (though this is unlikely). Therefore, we determine the 'true' orientation of the pin hole mask by creating a grid of positions, then compute

[1]available at http://www2.keck.hawaii.edu/inst/nirc2/preship_testing.pdf

[2]http://www.astro.ucla.edu/∼metchev/ao.html

the shift, scale and rotation which minimizes the residuals with the data in a least-squares sense. The best-fit scale differs from the nominal value of 39.686 mas/pix by only 5×10^{-4} and the best-fit rotation is 0.277° clockwise. For the narrow camera the best fit scale differs from the nominal value of 9.942 mas/pix by only 9.35×10^{-4} and it rotated 0.082° clockwise.

The residuals between the expected pin hole positions and the observed positions are shown in Figures 6 & 7 for the wide camera and in Figures 12 and 13 for the narrow camera. We see that the gross features are similar to the preship solutions, but there are some noticeable differences. We will quantify this below in § 5.

We fit a new polynomial solution using the same form as above for the measured and expected positions using the IDL package MPFIT by C. Markwardt [3]. For the wide camera we require a 3rd order solution whereas for the narrow camera a 4th order solution (and possibly higher) is justified. The solution can be found in Table 2. The 4th order polynomial is

$$\begin{aligned} x' &= a_0 + a_1 x + a_2 y + a_3 x^2 + a_4 xy + a_5 y^2 \\ &\quad + a_6 x^3 + a_7 x^2 y + a_8 x y^2 + a_9 y^3 \\ &\quad + a_{10} x^4 + a_{11} x^3 y + a_{12} x^2 y^2 + a_{13} x y^3 + a_{14} y^4, \end{aligned}$$

$$\begin{aligned} y' &= b_0 + b_1 x + b_2 y + b_3 x^2 + b_4 xy + b_5 y^2 \\ &\quad + b_6 x^3 + b_7 x^2 y + b_8 x y^2 + b_9 y^3 \\ &\quad + b_{10} x^4 + b_{11} x^3 y + b_{12} x^2 y^2 + b_{13} x y^3 + b_{14} y^4. \end{aligned}$$

The post-fit residuals are significantly improved. In the wide camera the RMS values in each axis are (σ_x, σ_y) = (0.0922,0.0870), $\lesssim 4$ mas. The residuals are shown graphically in Figure 8 and are broken down by coordinate in Figure 9. In the narrow camera we find post-fit residuals (σ_x, σ_y) = (0.0599,0.0639), $\sim 600\,\mu$as. The residuals are shown graphically in Figure 14 and are broken down by coordinate in Figure 15. Noticeable higher order structure remains in the narrow camera residuals, thus a higher order polynomial may further reduce the residuals.

5. Comparison with Pre-ship Solution

To compare the pre-ship solutions with our newly derived solutions we look at the predictions of both at a series of grid points over the chip. The residuals for the wide camera between the two solutions are shown in Figures 16 & 17 and in Figures 18 & 19 for the narrow camera. The most important difference is the appearance of an overall rotation between the new and pre-ship solutions for both the wide and narrow cameras. This likely stems from a small mistake in the pre-ship analysis. Namely, the *observed* pin hole positions were corrected for an overall rotation

[3] http://cow.physics.wisc.edu/ craigm/idl/idl.html

with respect to the NIRC2 axes (how this angle is measured is ambiguous) instead of the *expected* positions. This will yield a measurement of distortion that is about the right magnitude, but it will be associated with a slightly wrong portion of the chip.

We can remove this effect by computing a simple linear transformation between the two solutions (fitting for just shift, scale and rotation). The residuals after this computation (which is generally just an overall rotation) are shown in Figures 22 & 23 for the narrow camera and Figures 20 & 21 for the wide camera. The top and lower right-hand corners seem to show the most significant discrepancies when compared to the pre-ship values, ~ 1 pixel.

6. TBD

Some questions that still need to be answered:

- Is it correct? Compare with real data.
- Are there filter effects? Have the data in hand.
- Is there a time dependence? Have the data in hand.

Table 1. Pre-ship Distortion Solutions for NIRC2.

Coefficient	Narrow	Wide
a_0	(-2.72 ± 0.94)E-01	(4.06 ± 0.46)E-01
a_1	(1.0009 ± 0.0005)E$+00$	(1.0008 ± 0.0002)E$+00$
a_2	(5.08 ± 0.52)E-03	(-3.24 ± 0.23)E-03
a_3	(-5.52 ± 0.52)E-06	(-1.75 ± 0.33)E-06
a_4	(7.7 ± 6.4)E-07	(-5.6 ± 3.0)E-07
a_5	(5.37 ± 0.80)E-06	(10.00 ± 0.33)E-06
a_6	(-8.6 ± 2.6)E-09	(-6.8 ± 1.3)E-09
a_7	(-8 ± 25)E-10	(8 ± 12)E-10
a_8	(-6.1 ± 2.7)E-09	(-3.6 ± 1.2)E-09
a_9	(-4.4 ± 3.4)E-09	(9 ± 13)E-10
b_0	(1.68 ± 0.94)E-01	(3.4 ± 4.6)E-02
b_1	(1.6 ± 4.7)E-04	(2.1 ± 2.3)E-04
b_2	(1.0008 ± 0.0005)E$+00$	(9.9477 ± 0.0023)E-01
b_3	(2.1 ± 6.5)E-07	(-4.4 ± 3.3)E-07
b_4	(-9.93 ± 0.64)E-06	(-9.2 ± 3.0)E-07
b_5	(1.78 ± 0.80)E-06	(-1.57 ± 0.33)E-06
b_6	(-1.6 ± 2.6)E-09	(2 ± 13)E-10
b_7	(-2.8 ± 2.5)E-09	(2.6 ± 1.2)E-09
b_8	(-4 ± 27)E-10	(5 ± 12)E-10
b_9	(-1.2 ± 0.35)E-08	(5.9 ± 1.3)E-09

Table 2. New Distortion Solutions for NIRC2.

Coefficient	Narrow	Wide
a_0	1.30660E−02	−6.32775E−01
a_1	1.00116E+00	1.00258E+00
a_2	1.96010E−03	−1.07553E−03
a_3	−3.14182E−06	−8.44603E−07
a_4	−3.08788E−06	−8.66153E−07
a_5	5.59549E−06	1.03161E−05
a_6	−6.04724E−09	−2.80832E−09
a_7	6.53706E−10	2.11712E−12
a_8	−3.99943E−09	−8.90944E−10
a_9	−1.63796E−09	−3.14757E−11
a_{10}	−1.12204E−11	—
a_{11}	1.35291E−11	—
a_{12}	5.73354E−12	—
a_{13}	3.37186E−12	—
a_{14}	−8.50332E−13	—
b_0	2.06853E−01	2.17931E−02
b_1	1.75403E−03	−1.39196E−03
b_2	1.00129E+00	9.96806E−01
b_3	−1.91215E−06	−2.81300E−07
b_4	−1.16438E−05	−5.77556E−07
b_5	−2.51404E−06	−1.44116E−06
b_6	6.03978E−11	5.30766E−10
b_7	−3.24360E−09	4.39543E−09
b_8	−3.55861E−09	−3.07567E−10
b_9	−8.66718E−09	7.84907E−09
b_{10}	5.17175E−12	—
b_{11}	2.66960E−12	—
b_{12}	5.29880E−12	—
b_{13}	7.83758E−12	—
b_{14}	4.80703E−12	—

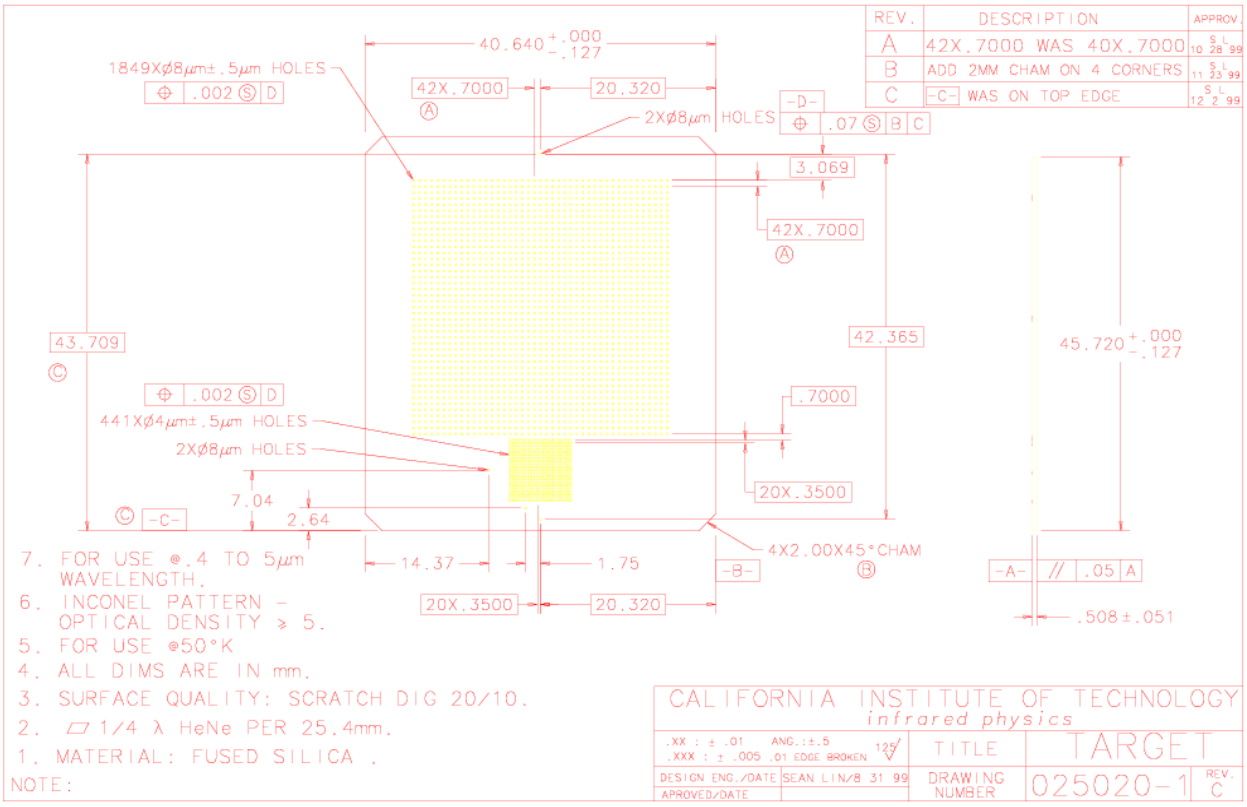

Fig. 1.— Schematic of the layout of the pin hole mask. All distances are in millimeters unless denoted otherwise (Courtesy K. Matthews).

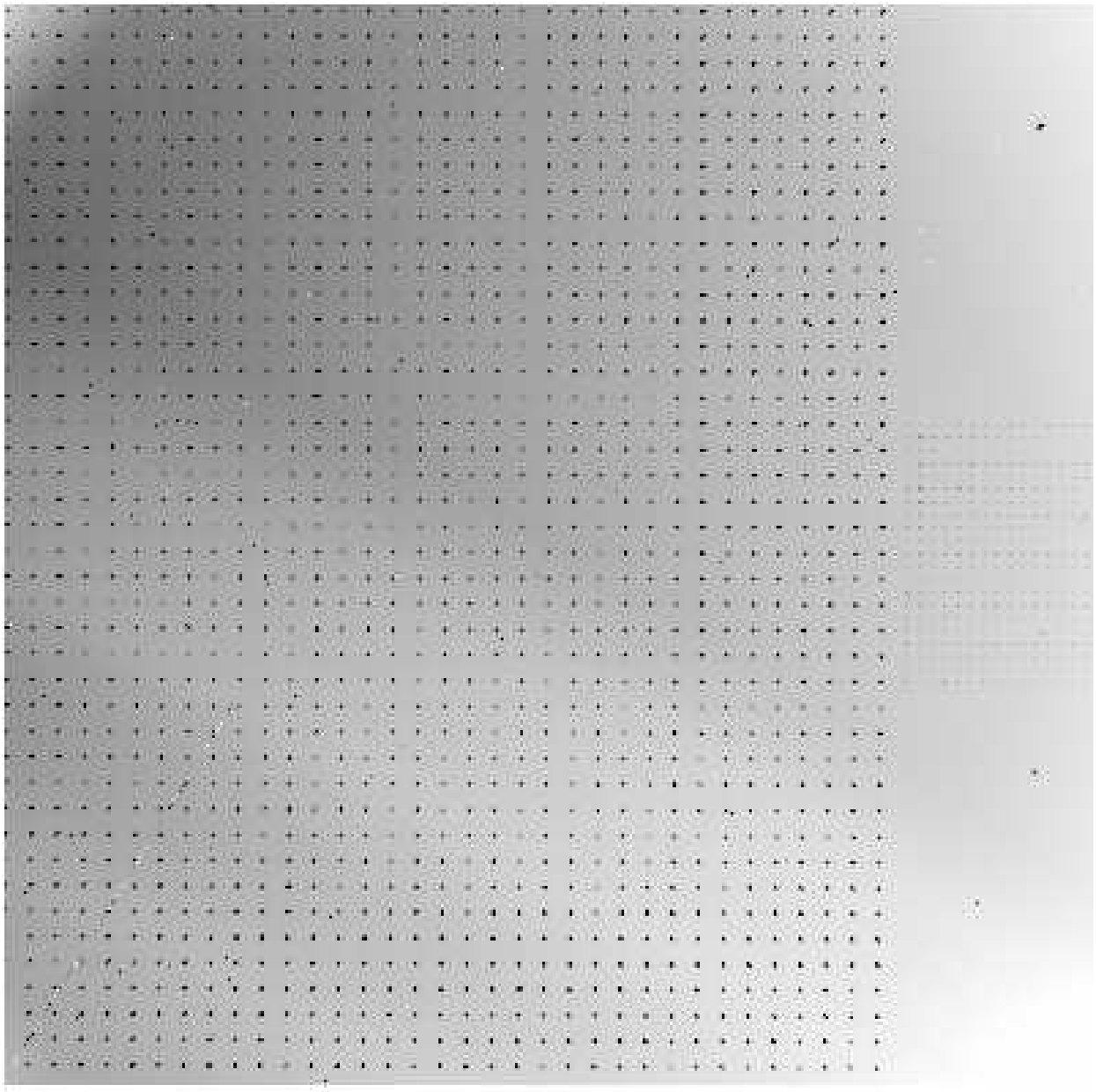

Fig. 2.— Image of the coarse pin hole mask with the wide camera. The gradient from poor flat fielding (due to light leakage) and the gap on the right section of the chip is evident (as is the fine mask).

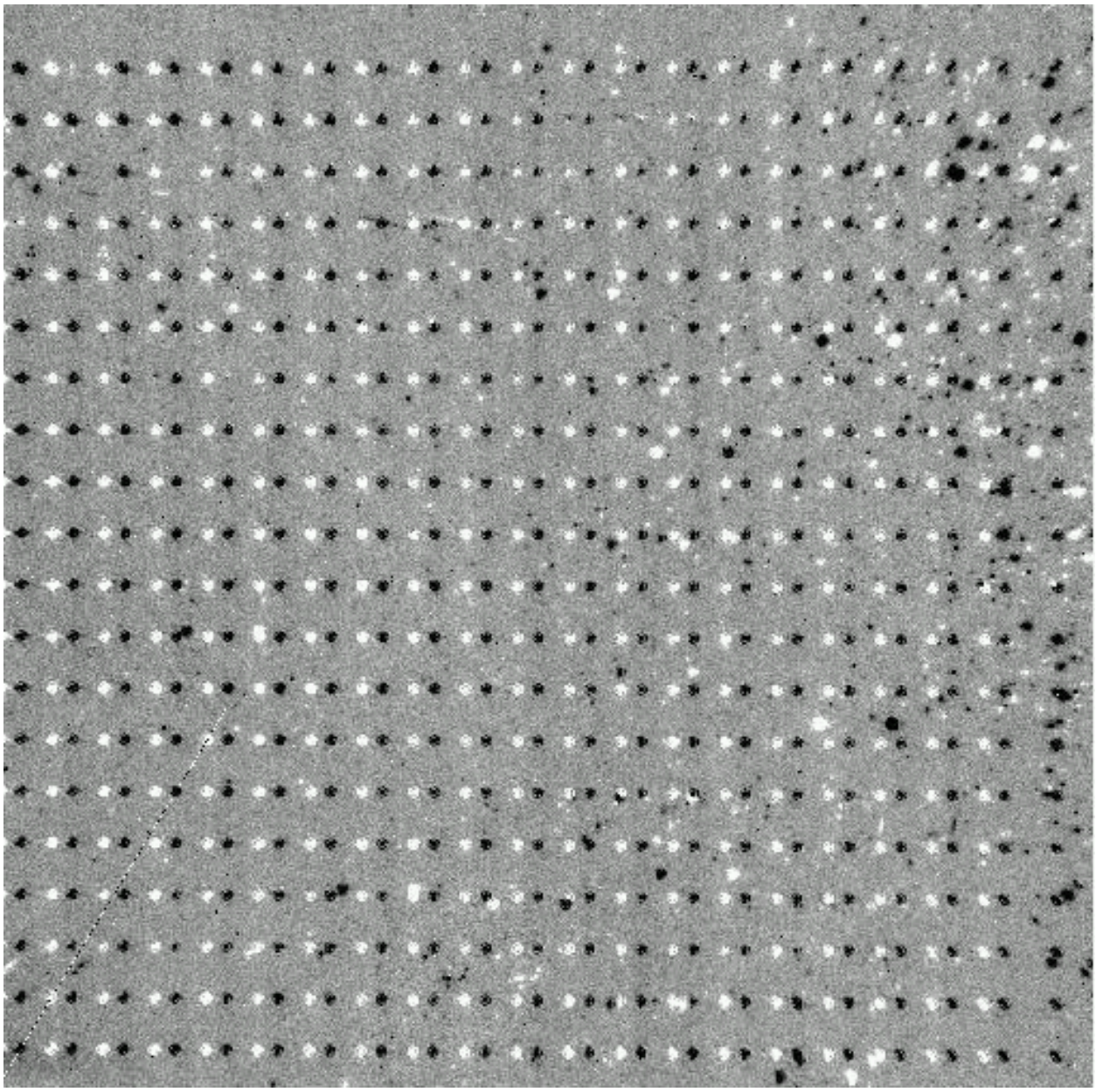

Fig. 3.— Difference image of two positions of the fine pin hole mask with the narrow camera. The artifacts on the right portions of the chip are likely due to defects in the mask substrate, but don't seem to significantly effect the determination of the pin hole source centers.

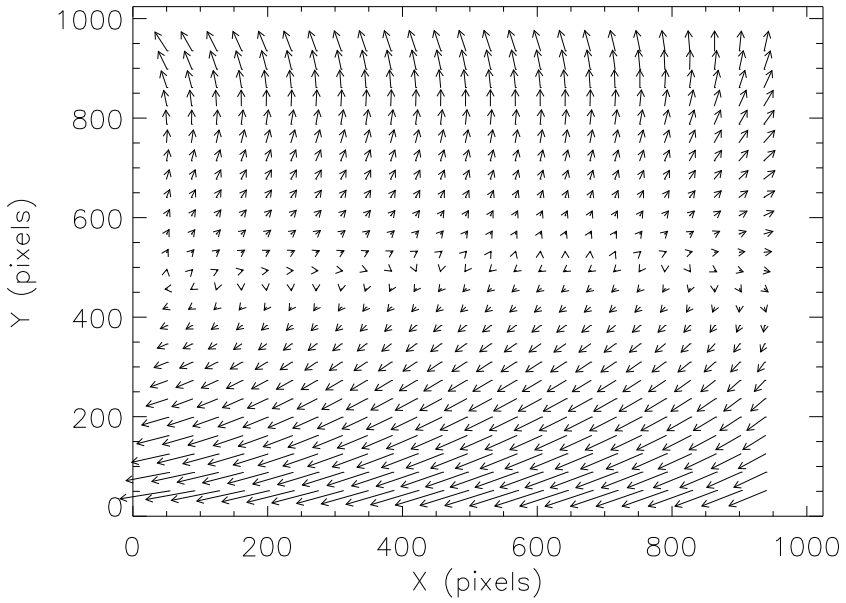

Fig. 4.— Distortion measured in the wide camera as reported by Thompson et al. See Figure 5 for the magnitude of the arrows.

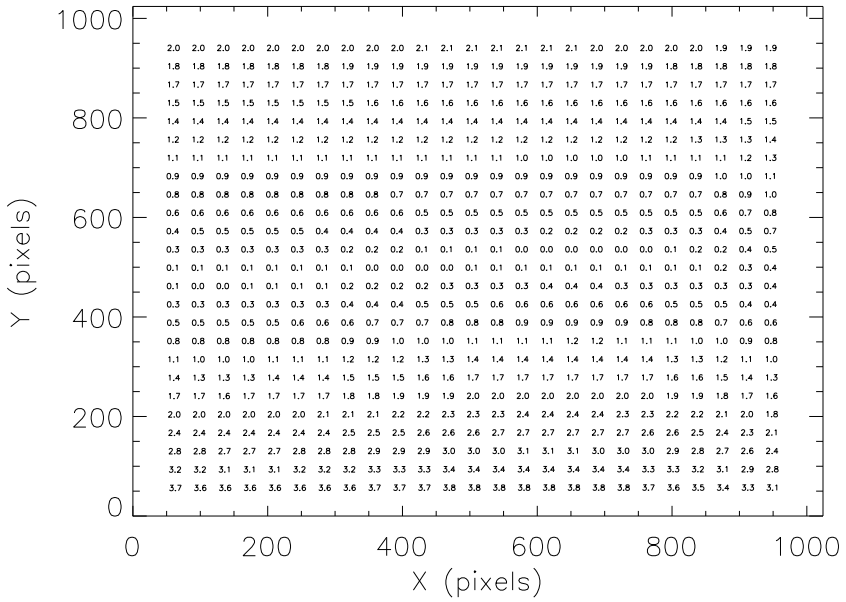

Fig. 5.— Amplitude in pixels of the pre-ship distortion in the wide camera.

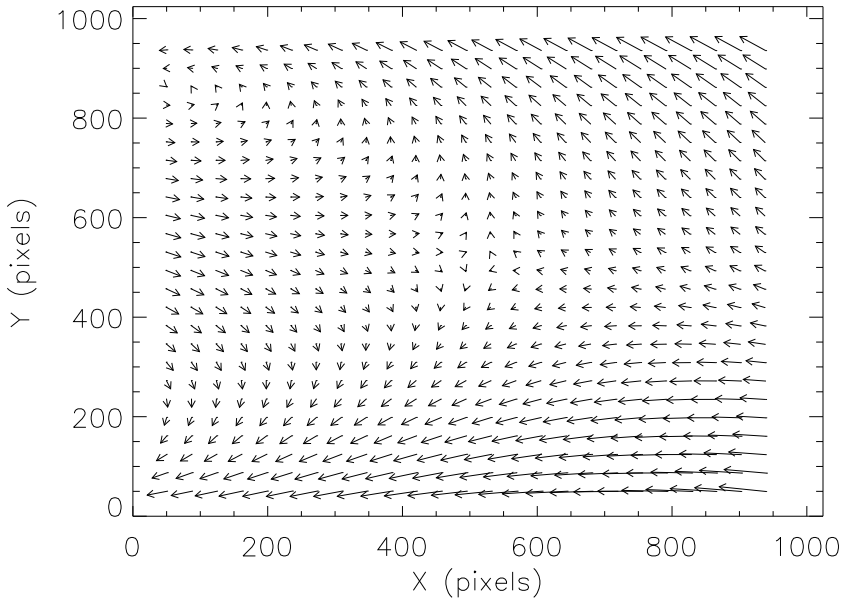

Fig. 6.— Distortion measured in the wide camera as measured in this work. See Figure 7 for the magnitude of the arrows.

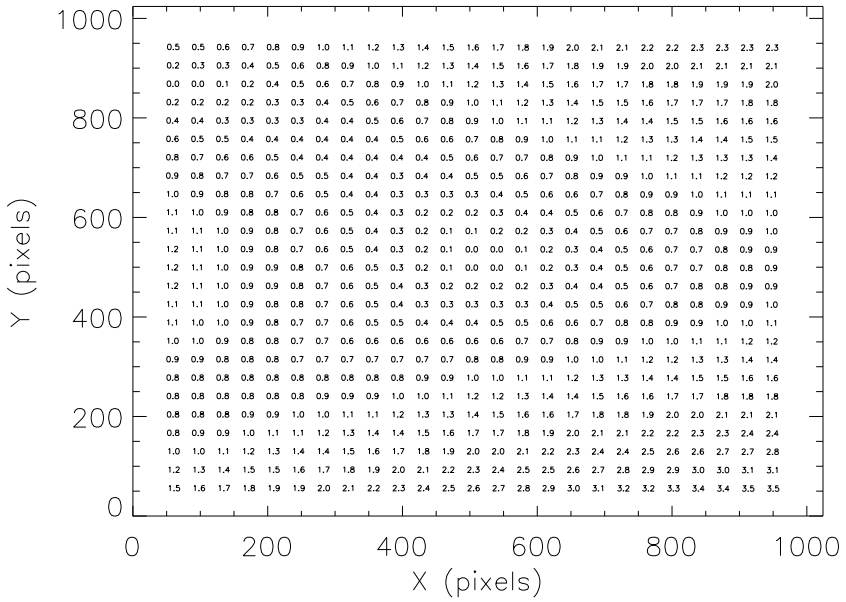

Fig. 7.— Amplitude in pixels of the distortion in the wide camera from the current data.

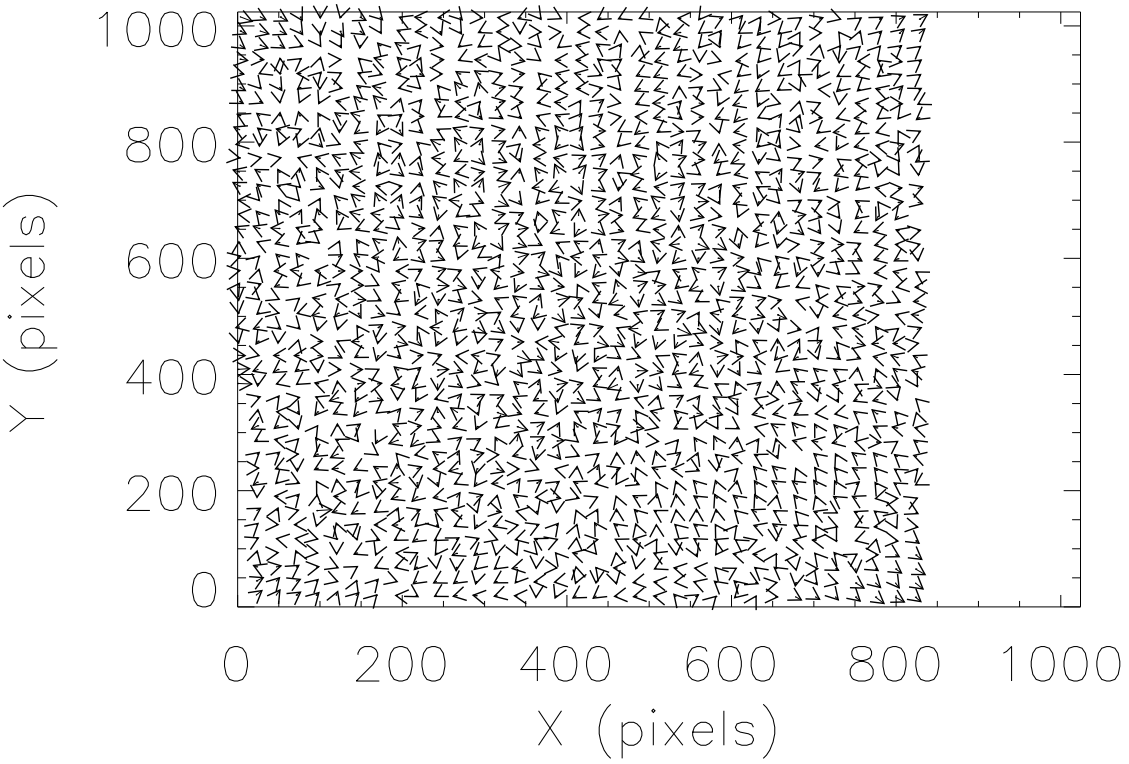

Fig. 8.— Measured residuals after application of the new wide camera distortion solution. Residuals are multiplied by a factor of 100. The residuals are < 0.1 pixels and do not show obvious systematic trends. See Figure 9 for further information.

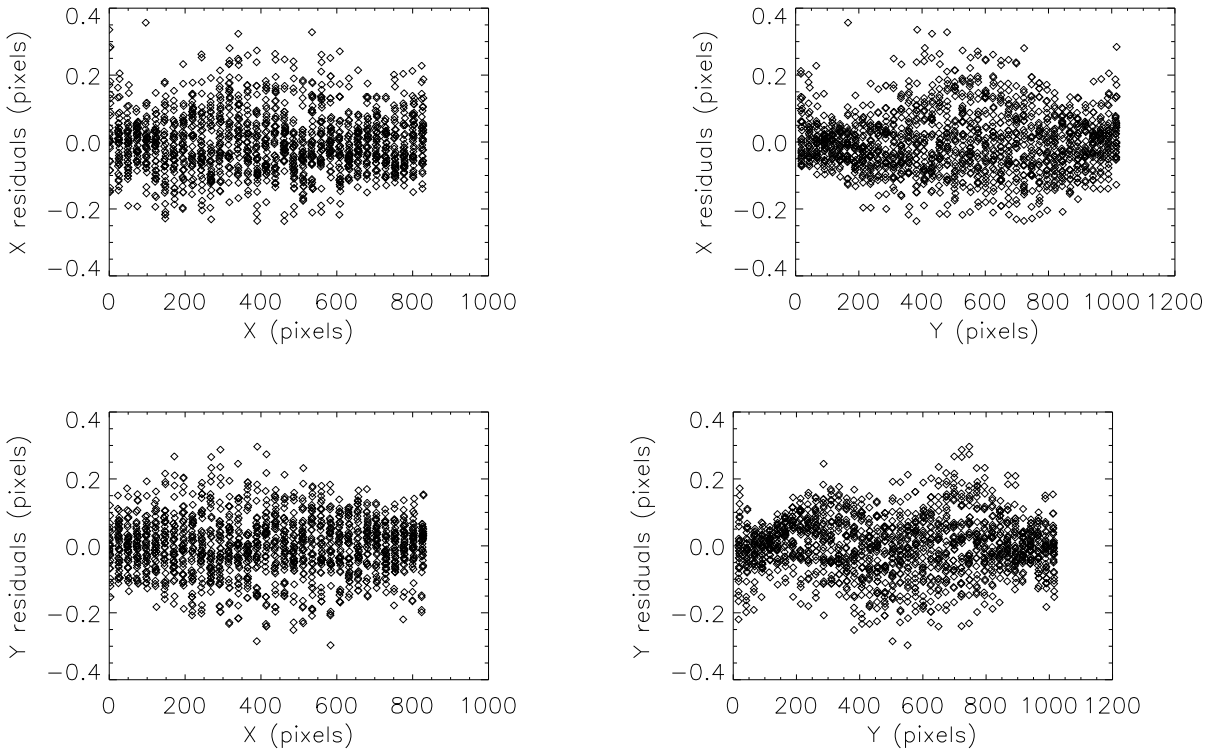

Fig. 9.— Wide camera residuals as a function of chip position. The RMS of the remaining residuals is $(\sigma_x, \sigma_y) = (0.0922, 0.0870)$ pixels. Includes all rows and columns.

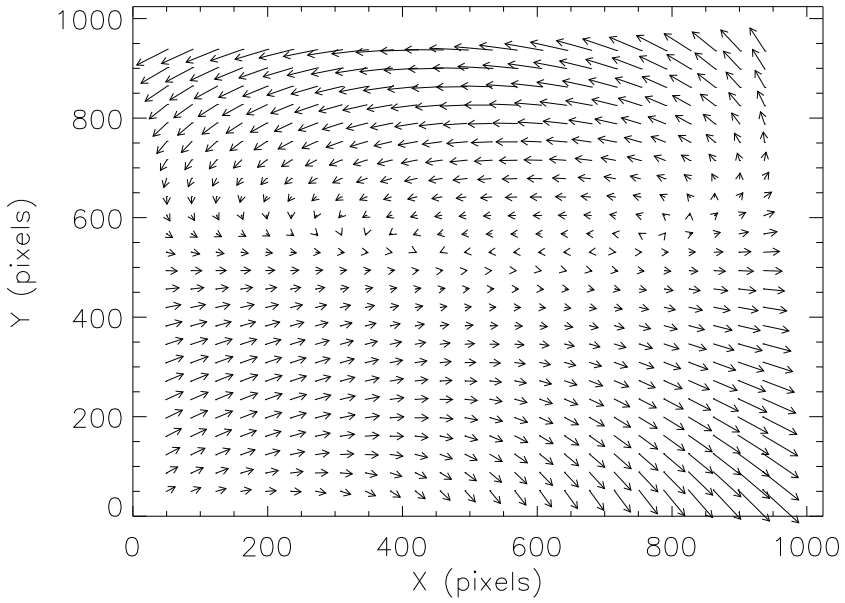

Fig. 10.— Distortion measured in the narrow camera as reported by Thompson et al. See Figure 11 for the magnitude of the arrows.

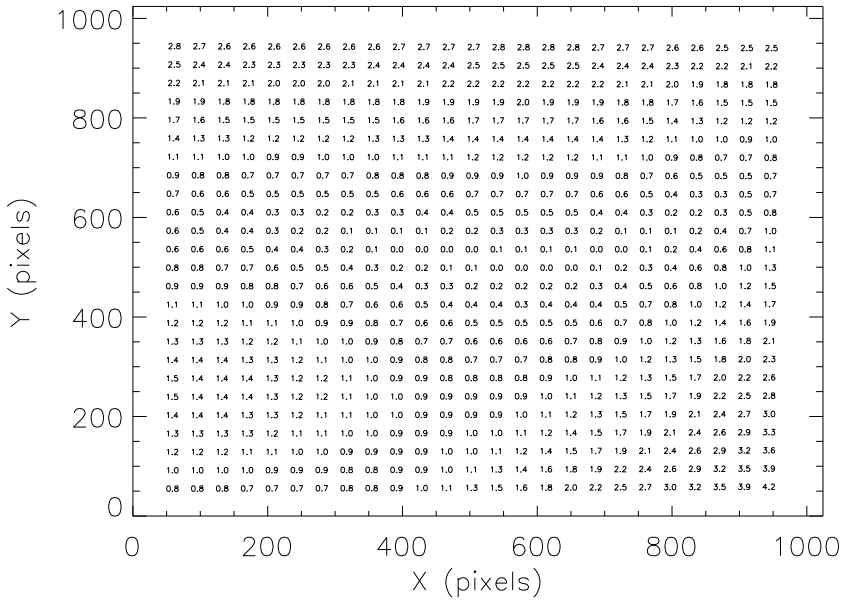

Fig. 11.— Amplitude in pixels of the pre-ship distortion in the narrow camera.

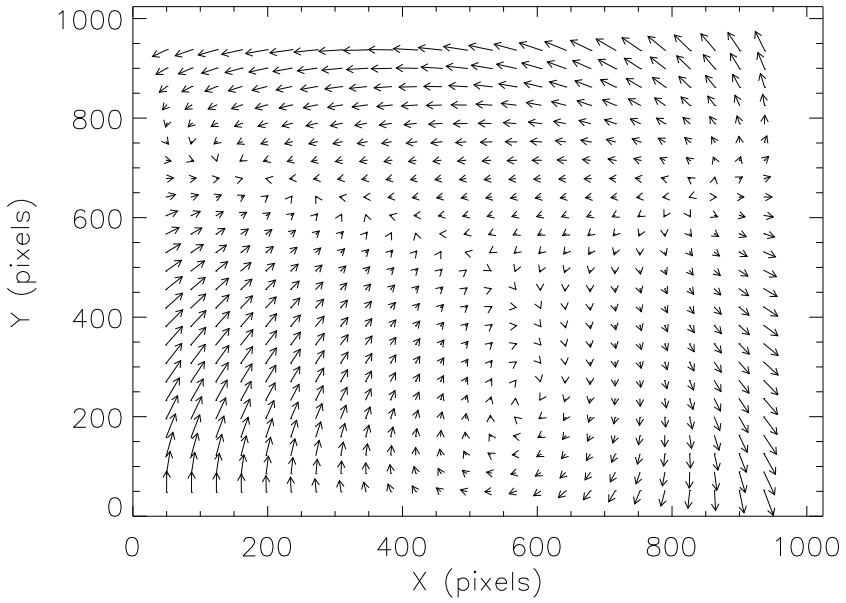

Fig. 12.— Distortion measured in the narrow camera as measured in this work. See Figure 13 for the magnitude of the arrows.

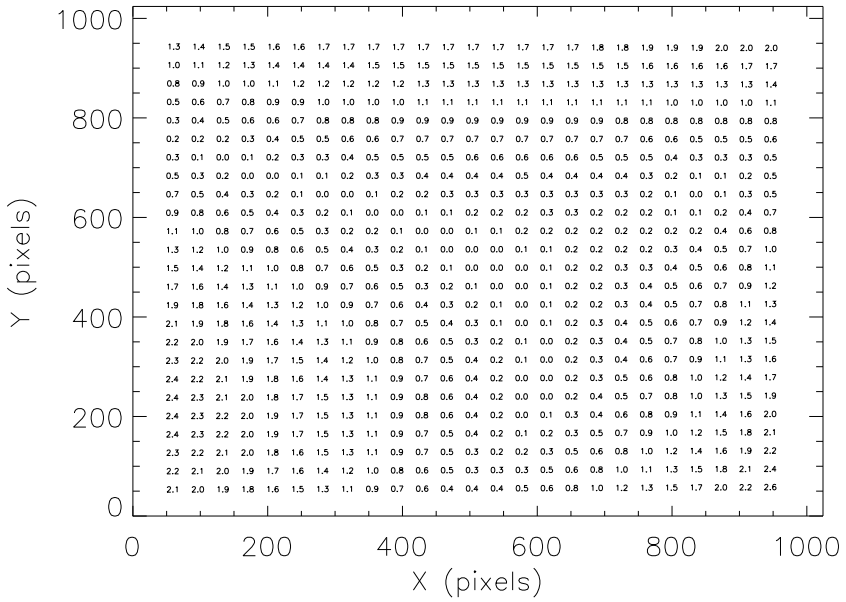

Fig. 13.— Amplitude in pixels of the distortion in the narrow camera from the current data.

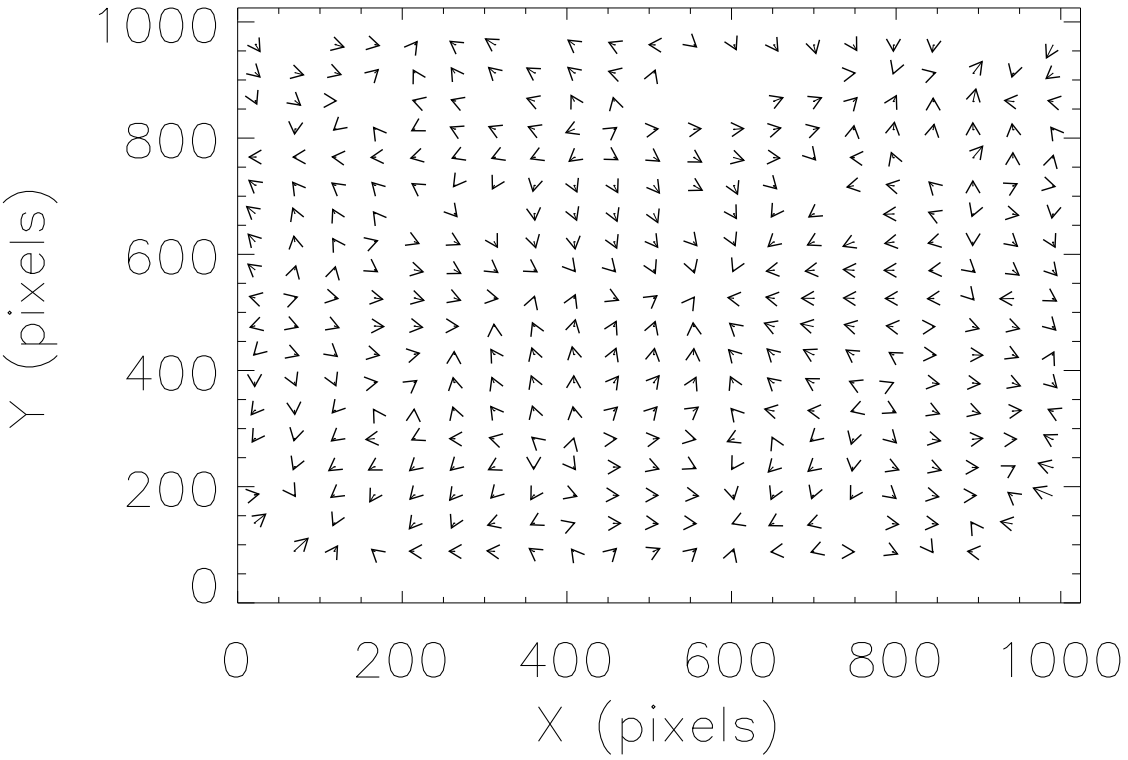

Fig. 14.— Measured residuals after application of the new narrow camera distortion solution. Residuals are multiplied by a factor of 100. The residuals are < 0.1 pixels and show some evidence for higher order trends. See Figure 15 for further information.

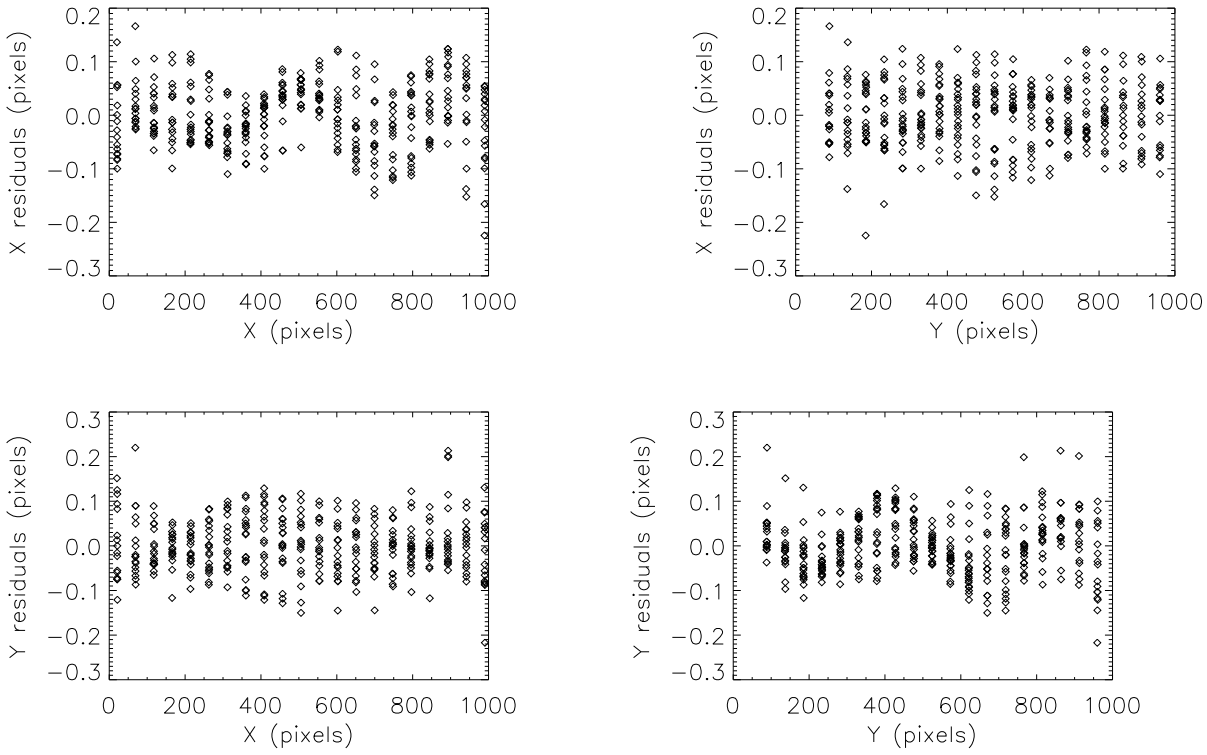

Fig. 15.— Narrow camera residuals as a function of chip position. The RMS of the remaining residuals is $(\sigma_x, \sigma_y) = (0.0599, 0.0639)$ pixels. Includes all rows and columns.

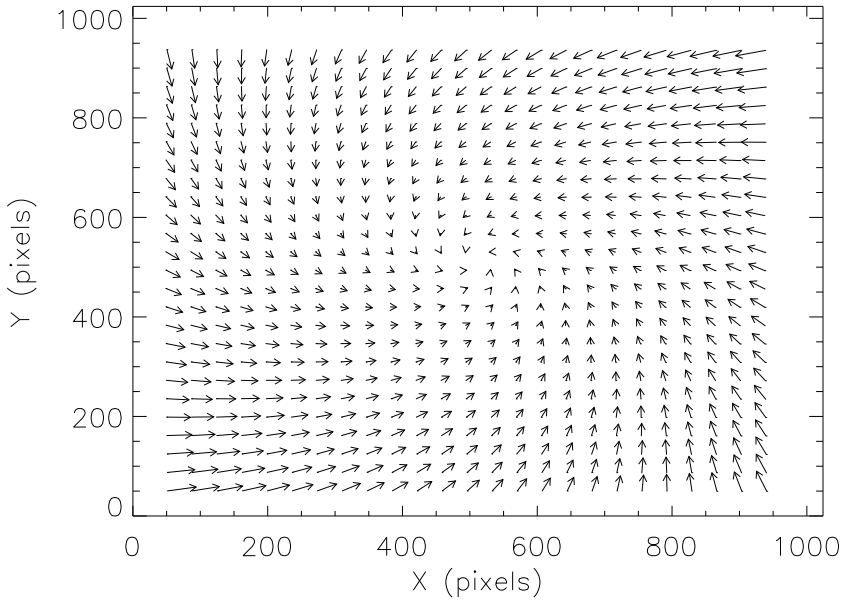

Fig. 16.— Comparison of the pre-ship and new wide camera distortion solutions. There appears to be an overall rotation of the two solutions with respect to each other. This is likely due to an incorrect procedure in determining the pre-ship distortion solution (see text for details).

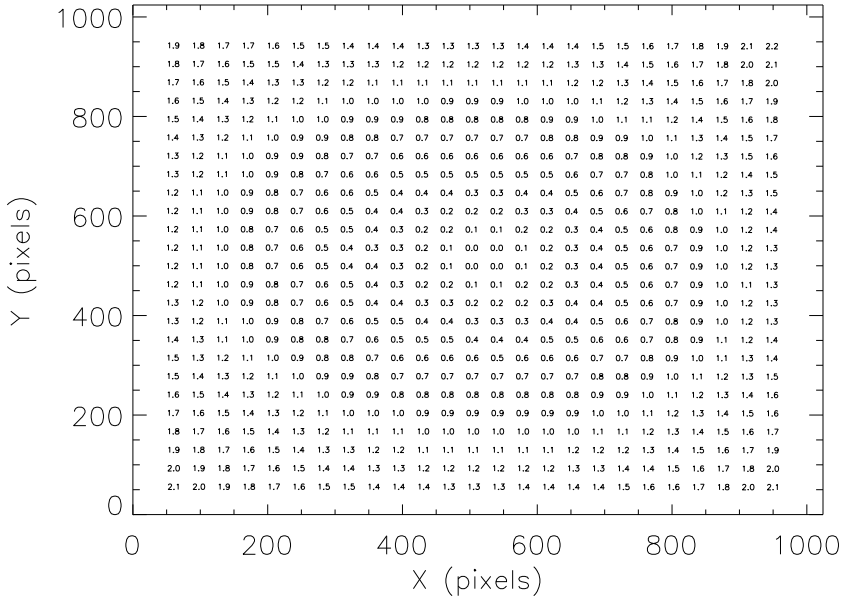

Fig. 17.— Amplitude of the arrows in Figure 16.

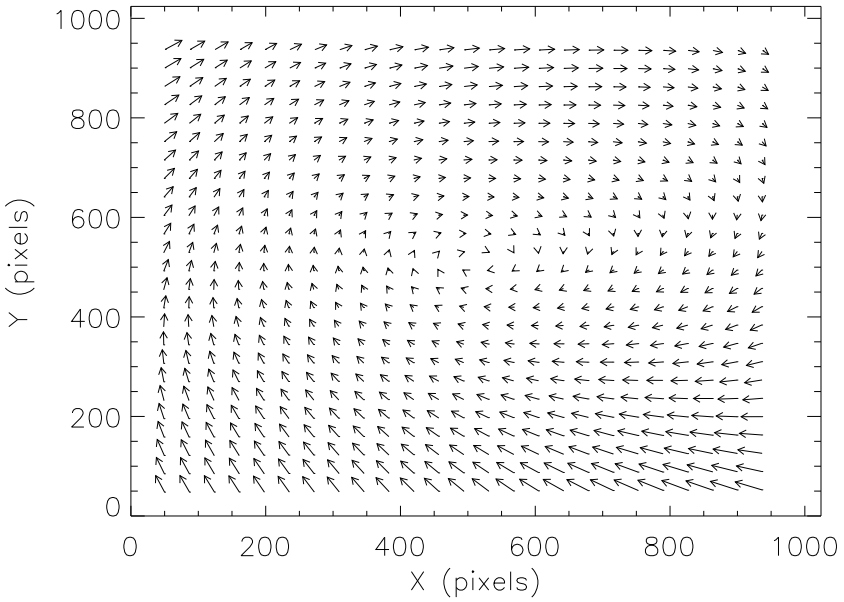

Fig. 18.— Comparison of the pre-ship and new narrow camera distortion solutions. There appears to be an overall rotation of the two solutions with respect to each other. This is likely due to an incorrect procedure in determining the pre-ship distortion solution (see text for details).

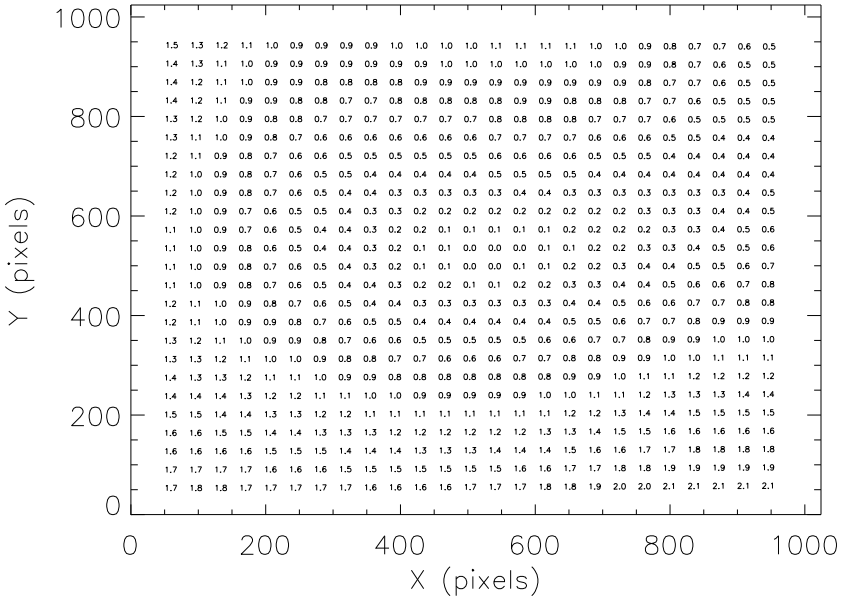

Fig. 19.— Amplitude of the arrows in Figure 18.

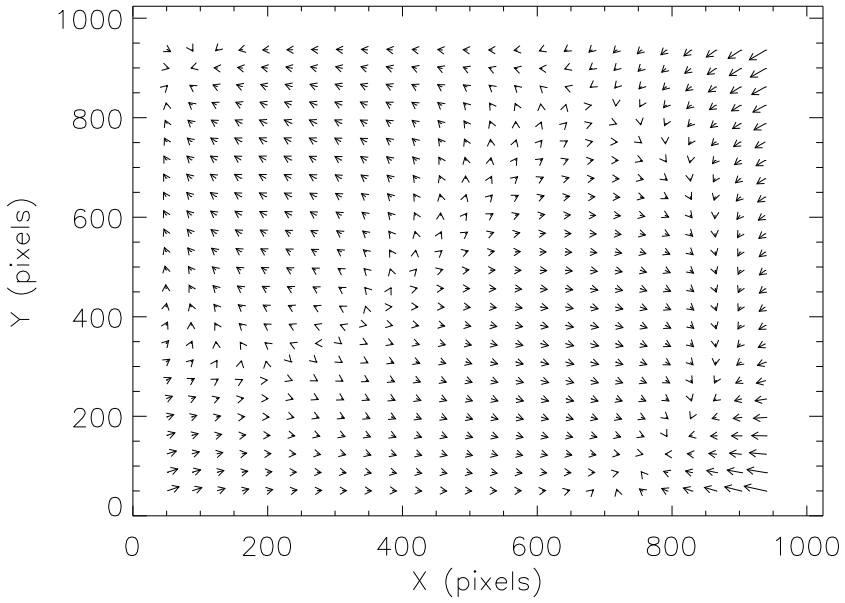

Fig. 20.— Comparison of the pre-ship and new wide camera distortion solutions after correcting for an overall shift scale and rotation. There are some small differences between the two solutions.

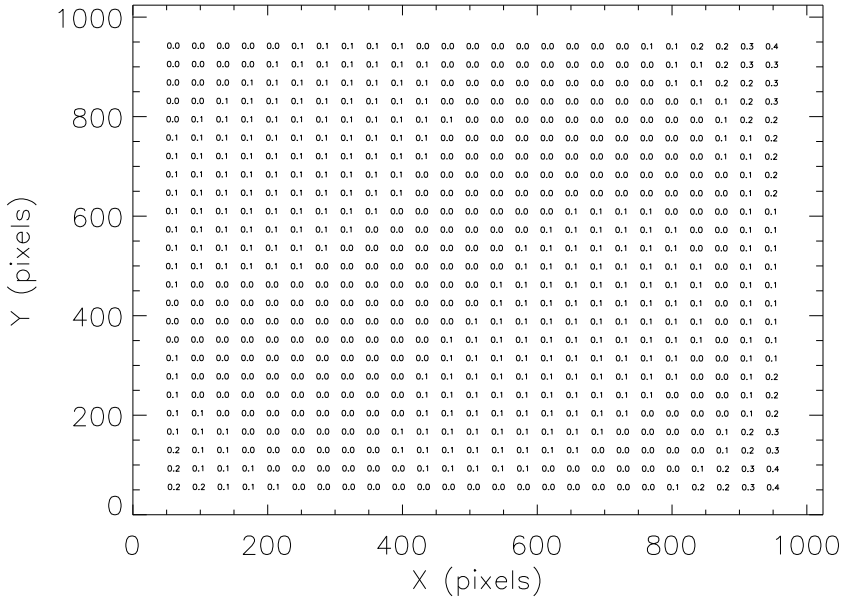

Fig. 21.— Amplitude of the arrows in Figure 20.

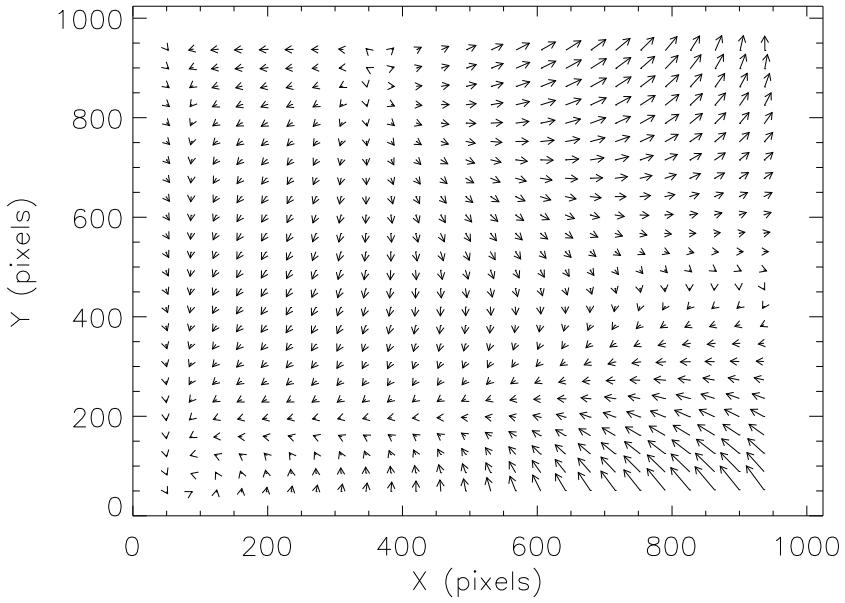

Fig. 22.— Comparison of the pre-ship and new narrow camera distortion solutions after correcting for an overall shift scale and rotation. There are some small differences between the two solutions.

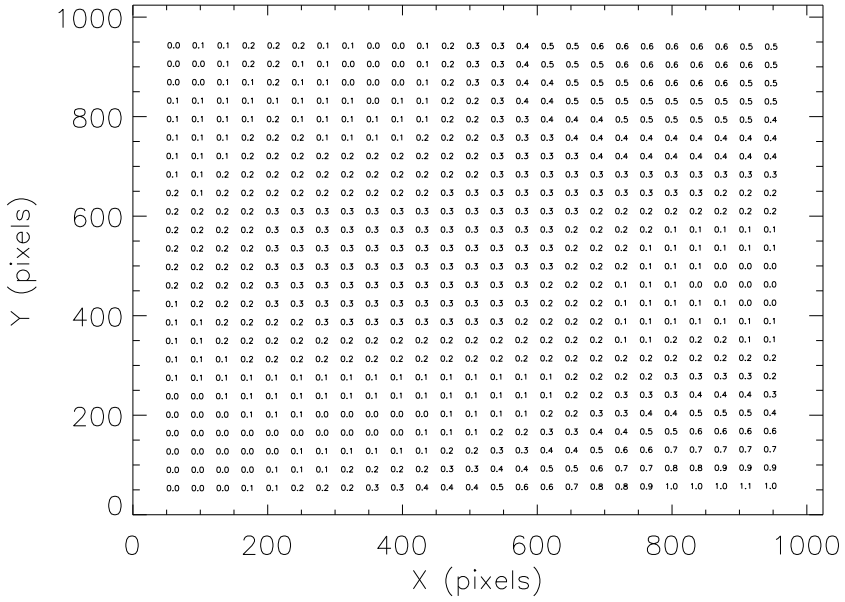

Fig. 23.— Amplitude of the arrows in Figure 22.